New theoretical instability regions and pulsational masses for blue large-amplitude pulsators

Daniel Jadlovský [ID],[1,2,3,4,*] Susmita Das [ID],[2,3,*] and László Molnár [ID][2,3,5]

[1]*Department of Theoretical Physics and Astrophysics, Faculty of Science, Masaryk University, Kotlářská 2, Brno, 611 37, Czech Republic*
[2]*Konkoly Observatory, Research Centre for Astronomy and Earth Sciences, HUN-REN, Konkoly-Thege Miklós út 15-17, H-1121, Budapest, Hungary*
[3]*CSFK, MTA Centre of Excellence, Budapest, Konkoly Thege Miklós út 15-17., H-1121, Hungary*
[4]*European Southern Observatory (ESO), Karl-Schwarzschild Str. 2, D-85748, Garching bei München, Germany*
[5]*ELTE Eötvös Loránd University, Institute of Physics and Astronomy, 1117, Pázmány Péter sétány 1/A, Budapest, Hungary*

ABSTRACT

Blue large-amplitude pulsators (BLAPs) are a recently discovered group of hot pulsating stars whose evolutionary status remains uncertain. We study the pulsation characteristics of BLAPs for the two main mass scenarios, $0.3 - 0.4$ M$_\odot$ and $0.7 - 1.1$ M$_\odot$, and compare them with observations to find evidence for either scenario. We compute about a half million linear BLAP models using MESA-RSP and compare the linear pulsation periods with the observed ranges of BLAP stars. For the low-mass scenario, BLAPs are in a region of the HR diagram where the growth rates are positive for the fundamental mode, and the model periods correspond well to the observed ones, assuming the reported luminosities of ~ 200 L$_\odot$. For the high-mass scenario, pulsations in the first overtone dominate. Assuming a larger range of luminosities, high-mass models could also explain all BLAPs, including the high-gravity BLAPs. Furthermore, we provide the first seismically constrained mass estimate for the first double-mode BLAP star, OGLE–BLAP–030. We find that a linear model with a mass of 0.62 M$_\odot$ matches the reported parameters of this star exactly, placing it in between the two mass scenarios. We also derive new period relations based on our models and all available observed BLAPs, and we find that the derived relations also support the low-mass scenario.

Keywords: blue large-amplitude pulsators – instability strip – MESA-RSP – pulsations

1. INTRODUCTION

Blue large-amplitude pulsators (BLAPs) are a new class of pulsating variables discovered recently by Pietrukowicz et al. (2017, hereafter P17), using the OGLE-IV survey (Udalski et al. 2015). BLAPs exhibit sawtooth-shaped light curves (see Fig. 1 of P17) similar to those observed in fundamental-mode RR Lyrae stars and classical Cepheids. However, they are found to have extremely short pulsation periods ($20 - 40$ min), high surface temperatures ($\sim$ 30000 K), large brightness variations (up to $0.2 - 0.4$ mag) and high surface gravity ($\log(g) \sim 4.5$). These parameters, therefore, place them in a region on the Hertzsprung-Russell diagram (HR diagram, see Fig. 7 of P17) not previously occupied by any known class of pulsating variables. The only other classes of variable stars nearby are the hot sub-dwarf stars (Heber 2016) or possibly

stars that belong to the extreme horizontal branch in globular clusters (Krtička et al. 2024).

After their discovery, further studies followed using complementary observations from the *Gaia* survey (Ramsay 2018; McWhirter & Lam 2022; Rimoldini et al. 2023; Gavras et al. 2023), the Zwicky Transient Facility (Kupfer et al. 2019, 2021; McWhirter & Lam 2022) and the Tsinghua University-Ma Huateng Telescopes for Survey (Lin et al. 2022, 2023a), among others. Furthermore, Kupfer et al. (2019) discovered BLAPs with surface gravities higher than (up to $\log(g) \sim 5.4$), and with periods shorter than ($\sim 2 - 8$ min) that of the original ones and classified these objects as high-gravity BLAPS (HG-BLAPS). More recently, dozens of new BLAPs were discovered in Outer Galactic Bulge and Galactic Disk using the OGLE-IV survey (Borowicz et al. 2023a,b; Pietrukowicz et al. 2024, hereafter P24).

So far, about 80 BLAP candidates have been discovered through the aforementioned photometric surveys (Borowicz et al. 2023b), and about a half of those have been spectroscopically confirmed (P17, Kupfer et al. 2019; Ramsay et al.

Corresponding author: Daniel Jadlovský, Susmita Das
jadlovsky@mail.muni.cz; susmita.das@csfk.org

* DJ And SD contributed equally to this work.

2022; Pigulski et al. 2022; Lin et al. 2023b; Chang et al. 2024; Bradshaw et al. 2024, P24).

Not much is known about the progenitors of BLAPs, but different evolutionary scenarios have been proposed. P17 suggested that BLAPs could be evolved low-mass stars with inflated envelopes. In particular, BLAPs are thought to be either helium-core burning stars with masses around $1.0\,M_\odot$ that have undergone significant mass-loss, or stripped red giants with masses around $0.3\,M_\odot$, in the pre-white dwarf stage, with hydrogen-shell burning above a degenerate helium core. Most follow-up studies that analyzed these scenarios further support the lower-mass scenario (e.g., Córsico et al. 2018; Romero et al. 2018; Kupfer et al. 2019; Byrne & Jeffery 2020; Byrne et al. 2021; Bradshaw et al. 2024), while a study by Wu & Li (2018) supported both scenarios. Paxton et al. (2019) reproduced light variability similar to the observed light curves for the higher-mass scenario. Alternatively, Xiong et al. (2022) proposed that BLAPs could be helium-shell burning stars with masses around $0.5\,M_\odot$. Zhang et al. (2023) also suggested that the BLAPs could be merger products.

Many of these scenarios rely on a binary evolution. However, as of now, only two BLAPs have been found to be a part of a binary system (Pigulski et al. 2022; Lin et al. 2023b), which is a major concern for these theories. Meng et al. (2020) and Meng & Luo (2021) suggested that BLAPs could be the survivors of a Type Ia supernova explosion of their companion, which could explain this observational discrepancy; the BLAPs produced by this configuration would have a mass of about 0.7 $M_\odot$.

Bradshaw et al. (2024) performed a full phase-resolved high-resolution spectroscopic analysis of a BLAP star for the first time and were able to determine its pulsation properties. They found large variations in radial velocity, temperature, and surface gravity. They found the best match for mass to be $\approx 0.3\,M_\odot$.

Recently, P24 analyzed 15 BLAPs with high-resolution spectroscopy. They confirmed that BLAPs form a homogeneous group in the period, surface gravity, and effective temperature spaces. However, they found two subgroups in terms of helium-to-hydrogen content, with the He-enriched BLAPs also being about five times more abundant in metals. They identified a multi-mode pulsator, OGLE–BLAP–030, with a fast period change. They also derived a period-luminosity and a period-surface gravity relationship based on their sample.

In this work, we use the Radial Stellar Pulsations (RSP) module of the open-source, state-of-the-art 1D code *Modules for Experiments in Stellar Astrophysics* (MESA; Paxton et al. 2011, 2013, 2015, 2018, 2019; Jermyn et al. 2023)[1]. The MESA-RSP package can be used to model large amplitude, self-excited, nonlinear pulsations of classical pulsators.

Paxton et al. (2019) showed that it can reliably produce the light curves of BLAPs. We therefore use MESA-RSP to explore the theoretical instability regions of the BLAPs in the HR diagram for the first time.

This paper is structured as follows: in Sec. 2, we describe the input parameters for the linear computation using MESA-RSP that we used to construct our grid of BLAP models. In Sec. 3, we present the edges of the instability regions exhibited by our BLAP models and compare the input stellar parameters with observed data. We directly compare our models against the new observations from P24 and try to find the best-matched model for OGLE–BLAP–030. Finally, in Sec. 4, we summarise our results.

2. DATA AND METHODOLOGY

In order to analyze the pulsation stability of a model, the MESA-RSP tool first builds an initial envelope model that is in static equilibrium. Afterward, a linear non-adiabatic (LNA) stability analysis of the envelope is performed, which provides its pulsation characteristics. Namely, we study periods and growth rates of the first three modes of radial pulsations in order to find the instability regions and their edges. We then compare various period relations with the observed data.

We constructed a very fine grid over the $ZXMLT_{\rm eff}$ parameter space with the following input parameters:

1. Stellar mass, $M = 0.3, 0.4, 0.7, 0.8, 0.9, 1.0, 1.1\,M_\odot$

2. Stellar luminosity, $\log(L/L_\odot) = 1.5 - 3.5$ in steps of $0.02\,L_\odot$

3. Chemical composition, $Z = 0.05, X = 0.7$

4. Effective temperature, $T_{\rm eff} = 20\,{\rm kK} - 35\,{\rm kK}$ in steps of 100 K.

This results in a combination of 106757 models per convection set. We used four default MESA-RSP convection sets (A, B, C and D, see Table 4 in Paxton et al. (2019)) that affect the energy transfer in the envelope. Thus, in total, our grid consists of about half a million models.

The selection of M was discussed in Sec. 1. For the L and $T_{\rm eff}$ ranges, we used data from P17 as an initial estimate, although the final ranges were determined from our testing before launching the main grid. For Z, as well as for other MESA-RSP parameters, we used the same settings as

---

[1] We used MESA version: MESA-r23.05.1, freely available at https:\github.com/MESAHub/mesa
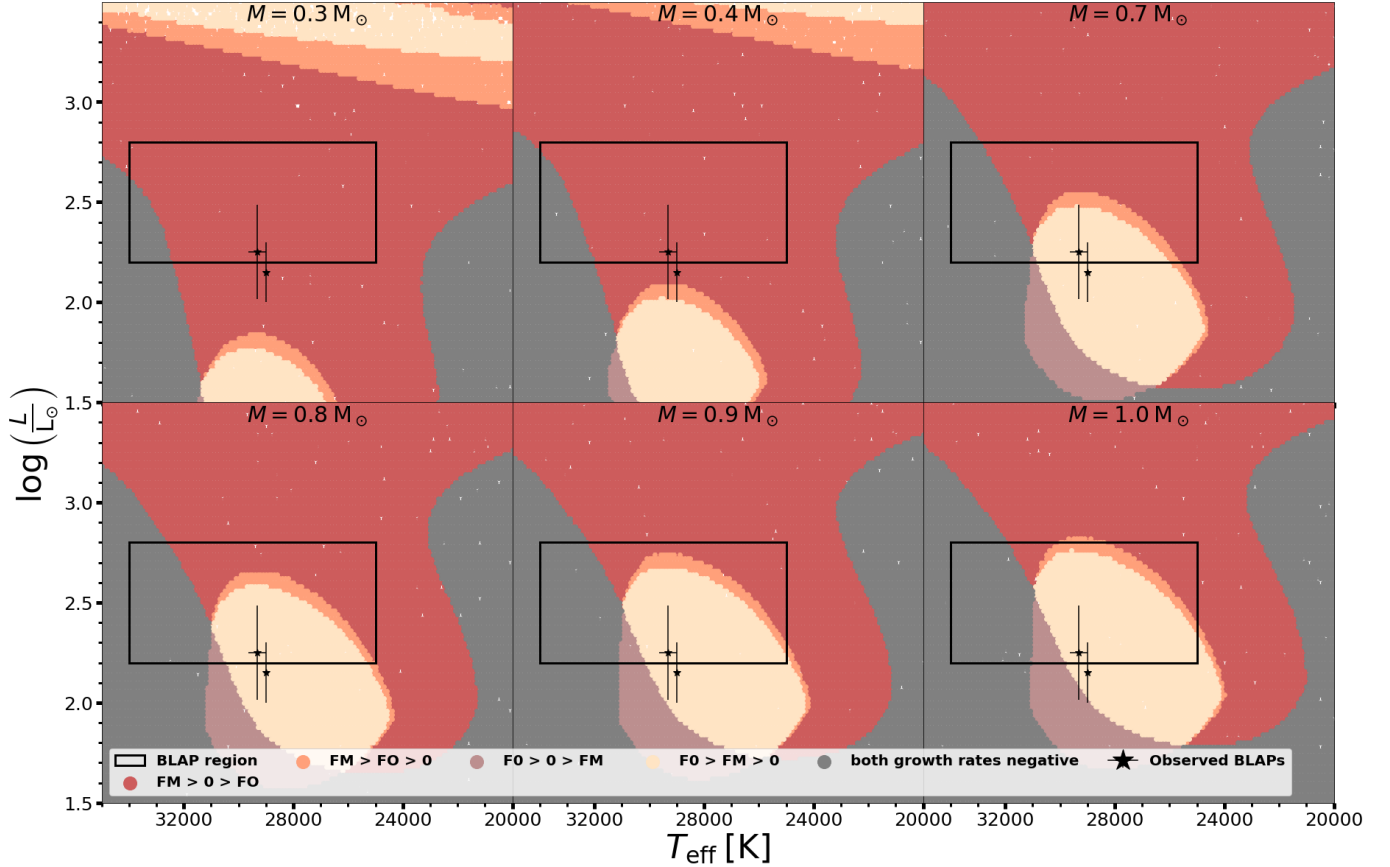
Figure 1. Instability regions for six different stellar masses computed using convective parameter set A. Red and magenta colors correspond to cases where only the FM or FO growth rates are positive, respectively. Yellow and orange colors indicate the areas where both mode growth rates are positive, with the FO or the FM being the stronger mode, respectively. The gray color corresponds to cases where neither of the growth rates is positive. The black square corresponds to an approximate location of BLAPs in the HR diagram based on P17; P24, whereas the black star symbols correspond to BLAPs for which L is determined observationally, from Pigulski et al. (2022) and Bradshaw et al. (2024). The plot demonstrates that the FO instability region moves to lower L for lower M. Additionally, the influence of MESA-RSP convective parameters is shown for $M = 1.1\,M_\odot$ in Appendix B, Fig. 5.

in Paxton et al. (2019). Therefore, N = 280, N_{outer} = 140, T_{anchor} = 2×10^5 K and T_{inner} = 6×10^6 K, as well as the relaxation conditions. An example inlist used for linear computations of the models using the convection parameter set A is provided in Appendix A. Similar inlists were used for the other three convection parameter sets.

Additionally, we constructed a second grid of models to match the observed properties of OGLE–BLAP–030 from P24 (see Sec. 3.3). For this purpose, we add stellar masses in the range $M/M_\odot \in \langle 0.6, 0.7 \rangle$ with a step of $0.01\,M_\odot$, stellar luminosities $L/L_\odot \in \langle 150, 300 \rangle$ with a step of $10\,L_\odot$, and effective temperatures $T_{eff} \in \langle 31100, 31700 \rangle$ K with a step of 50 K around the observed properties of the star and using a chemical composition of $Z = 0.05, X = 0.7$, and the convection parameter set A. This resulted in 2080 models.

3. RESULTS

In the following subsections, we analyze results from the LNA analysis for the fundamental mode (FM) and first overtone (FO).

3.1. *Instability region*

In Fig. 1, we present an overview of our results on the HR diagram, showing the positions of the linear instability regions for different masses. We can see that the FO region moves towards higher luminosities with increasing mass. For the low-mass scenario, the FO region has stellar luminosities too low to match the estimated BLAP region in the HR diagram. This demonstrates that the pulsation mode can help us differentiate between the two mass scenarios. In the part of the HR diagram where the BLAPs are found (based on literature values from P17; P24), the FO growth rates are dominant for the higher mass scenario (0.7 − 1.1 M$_\odot$). Whereas, for the lower mass scenario (0.3 − 0.4 M$_\odot$), the FM growth rates dominate and the FO is no longer excited.

Therefore, in the following sections of the paper, the FO periods of the higher mass scenario are compared with FM periods of the lower mass scenario, in order to determine which scenario corresponds better to the literature values for BLAPs. Furthermore, Fig. 1 also shows that the two BLAPs with observationally determined luminosities at $L \sim 200\,L_\odot$ (Pigulski et al. 2022; Bradshaw et al. 2024) lie at the bottom of the approximate BLAP region, which was estimated in earlier studies (e.g., P17), suggesting that the real L of BLAPs is lower than previously expected. Therefore, we focus on models with $L \sim 200\,L_\odot$ as the main candidates of BLAPs, although for comparison we also discuss models with other L, namely $\sim 400\,L_\odot$ (middle of the original estimated BLAP region).

As illustrated in Fig. 5 in Appendix B, we find that the choice of MESA-RSP convective parameters has a significant effect on the growth rates in different pulsation modes. The plots show that radiative cooling (set B and D) affects period growth rates the most, causing the instability region to become smaller. Nonetheless, for other physical parameters that we study in this paper, the choice of convective parameters gives only negligible difference. While a calibration of the convection parameters for BLAPs is indeed important, it is beyond the scope of this study. Therefore, for the subsequent analysis, we proceed with the linear models that were computed using the simplest convection parameter set A.

It is also worth noting that other types of pulsating stars may contaminate our instability region: another instability region is visible in the upper part of the HR diagram for lower masses in Fig. 1. Thus, even though some of our models may not be related to BLAPs, they could still represent other types of variable stars. They could correspond, for example, to various variable hot subdwarf stars with longer periods (e.g., Heber 2016; Krtička et al. 2024).

3.2. *Petersen diagram*

In Fig. 2, we show the Petersen diagram (Petersen 1973), the dependency of the ratio of two pulsation periods relative to the longer period, in this case, P_{FO}/P_{FM} on $\log(P_{FM})$. Mode period ratios depend strongly on the physical parameters of the stars and on the radial orders of the modes. As such, they are a powerful tool both for mode identification and for variable classification (see, e.g. Smolec et al. 2017; Netzel et al. 2022). Although only one double-mode BLAP has been discovered so far, we provide the Petersen diagrams for both mass scenarios to showcase where to expect such stars.

We compare models of different masses to the P_{FO}/P_{FM} mode period ratios for other groups of variable stars, as shown, for instance, in Pigulski (2014). The short periods where the pulsations in FM and FO are excited ($\log(P_{FM})$ from about -2 to -1.2) place the BLAPs to the left from the

other groups of classical pulsators (the closest group would be high-amplitude δ Scuti stars), while the period ratio values ($0.72 - 0.8$) suggest that both mass scenarios are related to sequences of other classical pulsators. Meanwhile, it is notable that the distribution of period ratios of our models is quite similar in shape to that of RR Lyrae stars.

3.3. *Fitting the observed properties of OGLE–BLAP–030*

P24 reported the discovery of the first BLAP pulsating simultaneously in the FM and FO (the third period is assumed to be non-radial pulsation). This discovery allows us to directly test the capabilities of MESA-RSP, as we can compare the P_{FO}/P_{FM} ratio from our models to the reported value. Double-mode stars elsewhere on the Petersen diagram were similarly compared to linear models by, e.g., Nemec et al. (2011); Smolec et al. (2016); Prudil et al. (2017), and more recently by Netzel & Smolec (2022) and Netzel et al. (2023).

To find the best-fitting model, we had to extend the mass range of the original grid of models, as the star fell in between the low- and high-mass model ranges. Therefore, we constructed a finer grid around the reported properties of OGLE–BLAP–030: $P_{FO}/P_{FM} = 0.762$, $T_{eff} = 31400 \pm 300$ K and $\log(g) = 4.85 \pm 0.05$, until we got a nearly exact match (Fig. 3). We find that the best-fitting model has the same parameters as the observational constraints, at $P_{FO}/P_{FM} = 0.762$, $T_{eff} = 31400$ K, and $\log(g) = 4.83$.

The best-fitting model has a mass of $M = 0.62\,M_\odot$ and a luminosity of $L = 220\,L_\odot$. This places the model into the FM-dominated instability region, but very near to the edge of the FO-dominated region, making the double-pulsations plausible, as the edges depend on the exact treatment of convective parameters, amongst other factors. More importantly, the mass we found places the star into the intermediate-mass zone, in between the two scenarios proposed by P17.

3.4. *Period relations*

In Fig. 4, we show several theoretical period relations for a range of stellar masses. Model sequences follow the mode with the highest growth rate, which leads to an FM–FO mode switch in the high-mass models around $\log(P) \approx 1.45$, or around $P = 28$ min. We also compare our models to observationally determined physical parameters of stars, namely from P17, Pigulski et al. (2022), Kupfer et al. (2019), Ramsay et al. (2022), Lin et al. (2023b), Pigulski et al. (2022), Chang et al. (2024), Bradshaw et al. (2024) and P24, hereafter referred to as "observed BLAPs". Furthermore, based on all these observations, we also derive new period relations and compare them against the relations from P24, which was made using a smaller sample of BLAPs. An overview of the relations is available in Table 1. A comparison between empirical relations derived in this work and the ones from P24 listed in the Table shows that the slope and intercept parameters of both relations are quite similar (differences in the
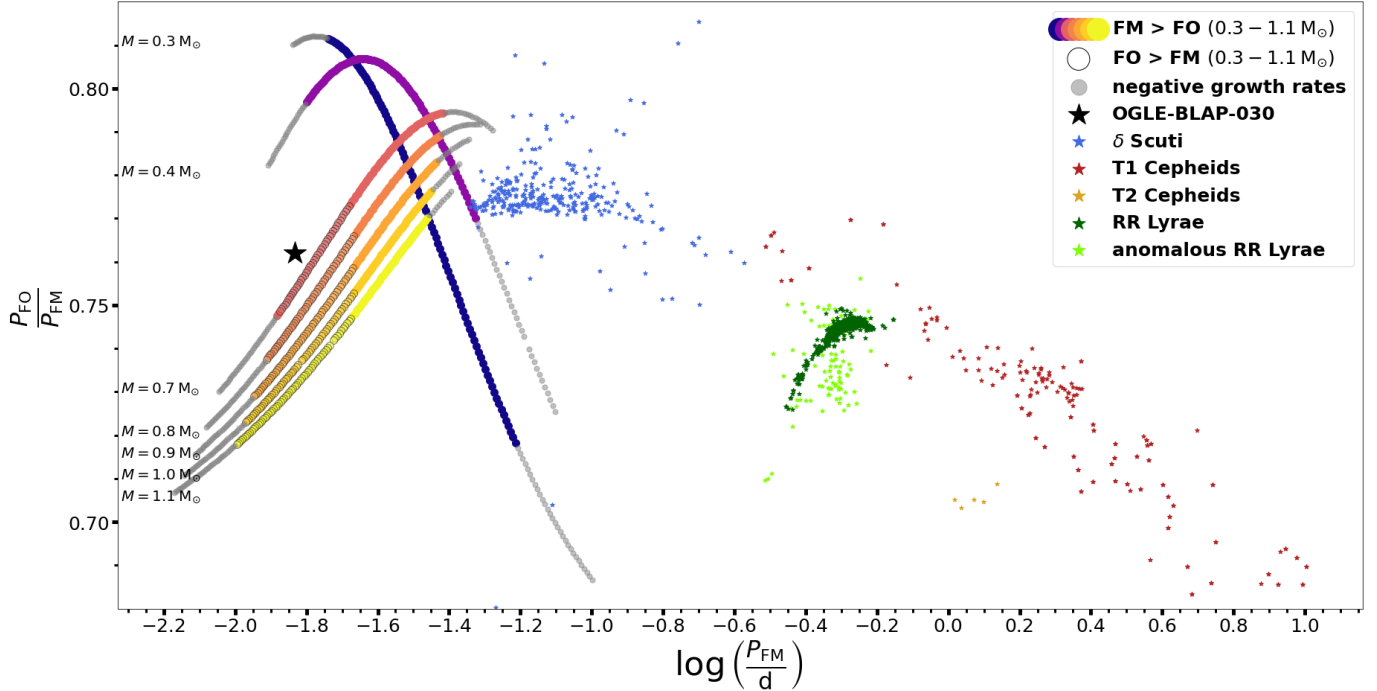
Figure 2. Petersen diagram: dependency of P_{FO}/P_{FM} over $\log(P_{FM})$ for seven different masses and for $L = 200\,\mathrm{L}_\odot$. BLAP sequences are color-coded with the mass. FO-dominated pulsations are present only for higher mass scenarios. The black star symbol corresponds to the position of the only known double-mode pulsator, OGLE–BLAP–030 (P24). In the figure, we also plot the P_{FO}/P_{FM} ratios for other groups of double-mode pulsator stars, namely δ Scuti (Netzel et al. 2022), Cepheids (Soszyński et al. 2015, 2020; Smolec et al. 2018; Udalski et al. 2018), and RR Lyrae stars (Soszyński et al. 2016, 2019).
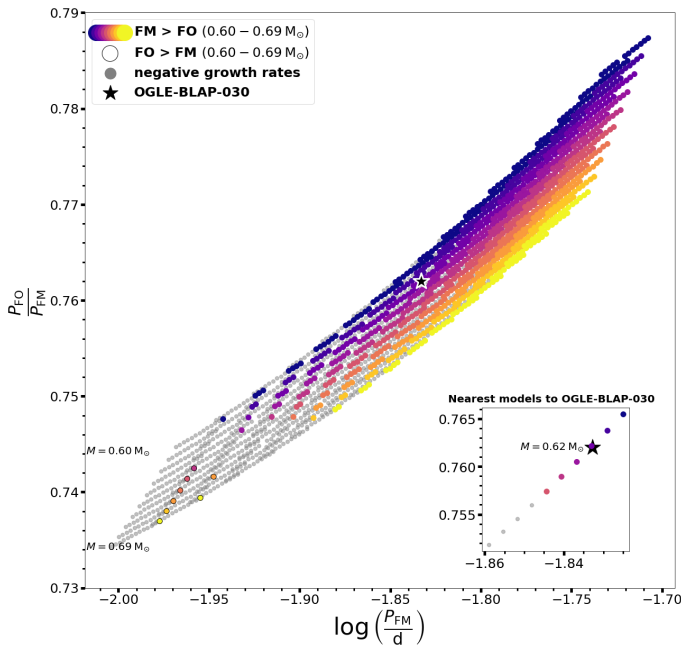
Figure 3. The same as Fig. 2, but for additional models between $M = 0.60 - 0.69\,\mathrm{M}_\odot$, which are closer to the observed period ratio of OGLE–BLAP–030. In the insert (with the ssame color coding), we only show models with the same T_{eff} and $\log(g)$ as reported for OGLE–BLAP–030 and which are close to the reported period ratio. From this, we get a nearly exact match for $M = 0.62\,\mathrm{M}_\odot$.

second decimal place). Likewise, a comparison between the theoretical relations obtained in this work and the empirical relations shows similar slopes in all the relations, except for the P-T_{eff} relation.

In Fig. 4a, we compare the observed periods and T_{eff} values with our results. The plot demonstrates that there is no shared observational P-T_{eff} relation for all BLAPs, which suggests that BLAPs consist of more diverse groups of stars, possibly at different stages of evolution. For low luminosities ($L \sim 200\,\mathrm{L}_\odot$), where two BLAPs have been observed by Pigulski et al. (2022); Bradshaw et al. (2024), the low-mass scenarios and corresponding FM periods clearly agree with observed T_{eff} values more than the FO periods for the higher-mass scenario do, as the periods would be too short for the latter case. Nonetheless, the FO models could correspond to the HG-BLAPs, assuming an even lower $L \sim 100\,\mathrm{L}_\odot$ (the same would be the case of low-mass models, but only for extremely low luminosities of $L < 50\,\mathrm{L}_\odot$). Alternatively, assuming a higher L of $\sim 400\,\mathrm{L}_\odot$, the situation becomes very favorable for the FO periods of the high-mass scenarios (as well as their FMs), which would correspond to the observed periods of BLAPs better. At those luminosities, the FM periods of the lower-mass scenario would become too long to match the BLAPs.

In Fig. 4b, we show the period-luminosity relation for the models. The two BLAPs with observationally determined lu-
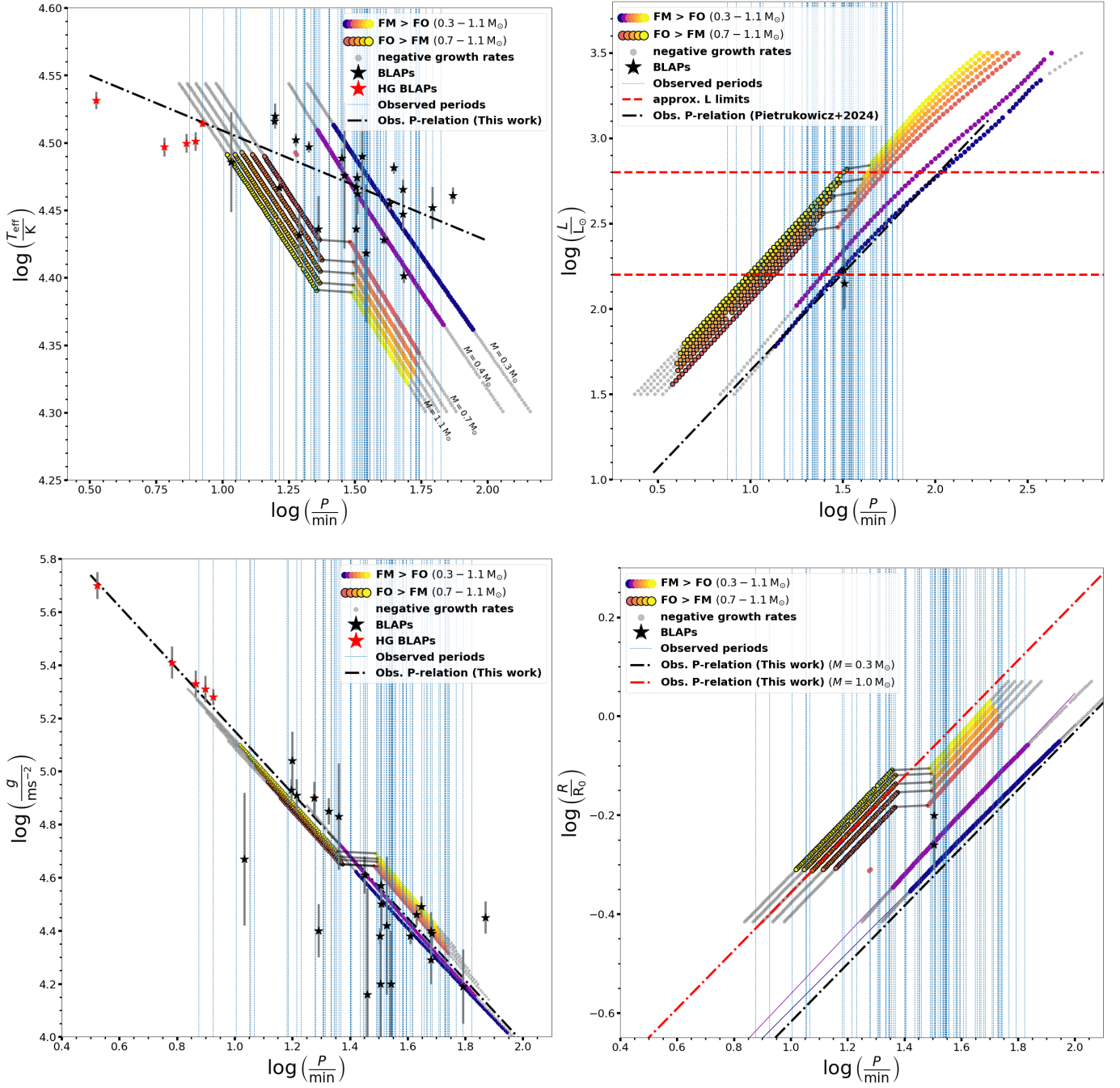
Figure 4. Comparison of observed BLAPs with the results from LNA analysis for seven different values of mass (mass color coding in all four panels is the same as in the first plot), showing various period relations. The FM–FO transition for the higher-mass models is marked with grey lines. Where physical parameters are available for the observed BLAPs, we show their positions with black and red star symbols, otherwise, when only the periods are known, we mark the period values with blue dashed lines across the plots. We also plot the determined observed period relations, including the period-luminosity relation by P24. *a)* P-T_{eff} relation, for $L = 200 \, L_\odot$. *b)* P-L relation, for $T_{\text{eff}} = 29800 \, \text{K}$, which is roughly an average of all BLAPs with known T_{eff}. *c)* P-log(g) relation, for $L = 200 \, L_\odot$. *d)* P-R relation, for $L = 200 \, L_\odot$. The observed relations were calculated using $R = \sqrt{\frac{GM}{g}}$ based on our P-log(g) relation, for two values of mass. The plot also includes both values of R determined by Bradshaw et al. (2024) for OGLE–BLAP–009.

minosity (Pigulski et al. 2022; Bradshaw et al. 2024) agree more with the low-mass scenario. Likewise, P24 derived a *P-L* relation based on the physical characteristics of a well-constrained star, OGLE–BLAP–009 (the same star as in Bradshaw et al. 2024). This relation also agrees with the low-mass scenario, suggesting that OGLE–BLAP–009 is indeed a low-mass BLAP. However, more independent luminosity determinations will be needed to constrain the mass dependence of the *P-L* relation.

In Fig. 4c, we show a *P*-log(*g*) relation. Here the scenarios are more difficult to disentangle. While the low-mass models can explain the BLAPs with the lowest log(*g*), it appears that there is another group of BLAPs with mid-range values of log(*g*) ~ 4.9, which cannot be explained by the same models, assuming $L \sim 200 \, L_\odot$ (unless a lower *L* is used). For the high-mass models, the situation is similar as it was for *P-T*$_{\rm eff}$ relations, i.e., models with higher *L* would match the observations well, while models with very low *L* could explain the HG-BLAPs. The period relations of both groups appear close to each other, although the exact parameters of observed period relations in Table 1 agree better with the low-mass scenario. Additionally, in the plots, we marked OGLE–BLAP–044 as an HG-BLAP, because its properties are quite close to this group (also discussed by P24), which can be clearly seen in Fig. 4c, where OGLE–BLAP–044 is the red point with the longest period.

Lastly, in Fig. 4d, we show the *P-R* relation. It is not possible to directly compare this plot with observations except for OGLE–BLAP–009 (Bradshaw et al. 2024), which is closer to the low-mass scenario. We calculated *P-R* using $R = \sqrt{GM/g}$, based on the observational *P*-log(*g*) relation, assuming $M = 0.3 \, M_\odot$ for the low-, and $M = 1.0 \, M_\odot$ for the high-mass scenarios. In both cases, the relation supports the respective mass that was used to calculate it, therefore we are not able to support either scenario.

Interestingly, all four plots also show that HG-BLAPs are at the edge of our parameter space, although they could be explained by high-mass scenario FO models with very low luminosities ($L \sim 100 \, L_\odot$), as we discussed. Figs. 4c and 4d also suggest that HG-BLAPs follow the same relations as normal BLAPs, extending them into higher values of log(*g*) and lower values of log(*R*). Thus, HG-BLAPs would be more compact objects than normal BLAPs.

4. CONCLUSIONS

We conducted an analysis of pulsation characteristics over a large grid of linear BLAP models in MESA-RSP. We used *ZXMLT*$_{\rm eff}$ physical parameter ranges claimed to correspond to BLAPs in order to test which of the proposed scenarios in the literature is correct.

1. Based on our models, there exists an instability region in the same part of the HR diagram where the BLAPs are located observationally. In this region, pulsations in both the FM and FO modes are present for the higher-mass scenario ($0.7 - 1.1 \, M_\odot$), with the FO mode dominating. For the lower-mass scenario ($0.3 - 0.4 \, M_\odot$), the FO strip moves to lower luminosities, hence only FM pulsations are present.

2. We predict the $P_{\rm FO}/P_{\rm FM}$ period ratios for double-mode BLAP stars. The two mass scenarios largely separate on the Petersen diagram and can offer a way to determine the preferred mass ranges.

3. Assuming a low *L* of ~ 200 $L_\odot$ (reported by Pigulski et al. 2022; Bradshaw et al. 2024), the FM periods of the low-mass models agree with the observations better, as well as with the empirical relations, most importantly with the *P-L* relation from P24. Likewise, the other period relations—*P-T*$_{\rm eff}$, *P*-log(*g*) and *P-R*—largely support the low-mass scenario models. However, the low-mass scenario does not appear to be able to explain the HG-BLAPs.

4. Assuming a higher *L* of ~ 400 $L_\odot$ (closer to the BLAP region estimated in earlier studies, e.g., P17), the high-mass models pulsating in the FO (and some in FM) could explain the observed BLAPs as well.

5. While our models did not fully explore physical parameters corresponding to HG-BLAPs, a comparison with our models demonstrates that HG-BLAPs are more compact objects with lower luminosities. They are close to our high-mass scenarios, where the FO pulsations dominate and where periods are short enough to correspond to the HG-BLAPs, assuming $L \sim 100 \, L_\odot$.

6. We validate our MESA-RSP pulsation models against OGLE–BLAP–030, the first multi-mode pulsator discovered by P24. Based on the observed FO/FM period ratio, $T_{\rm eff}$, and log(*g*), we find a model with exactly the same parameters. This uniquely allows us to determine the mass and luminosity of OGLE–BLAP–030 as $M = 0.62 \, M_\odot$ and $L = 220 \, L_\odot$, placing it into the mid-mass range. Our model is located near the edge of the FM/FO-dominated region, making the multimode pulsations plausible. The high observed period change (P24) of the star suggests that it is evolving from/towards one of our BLAP groups.

7. The choice of convective parameters strongly affects the growth rates, especially the addition of radiative cooling (set B and D), which affects the shape of the instability strip more than the addition of turbulent pressure and flux (set C). However, a calibration of the convection parameters for the atmospheres of BLAPs has

Table 1. Theoretical period relations derived in this study (for $T_{\rm eff}$ = 29800 K in the case of P-L relation and for L = 200 $L_\odot$ for the rest) and their comparison to the observed relations. For theoretical relations, the errors are all about or smaller than < 0.01. For empirical relations, they are written as subscripts.

M [$M_\odot$]	$\log\left(\frac{L}{L_\odot}\right)$	$\log\left(\frac{T_{\rm eff}}{K}\right)$	$\log\left(\frac{g}{{\rm ms}^{-2}}\right)$	$\log\left(\frac{R}{R_\odot}\right)$
Theoretical relations				
0.3 FM	$1.06\log\left(\frac{P}{\min}\right)+0.63$	$-0.29\log\left(\frac{P}{\min}\right)+4.92$	$-1.15\log\left(\frac{P}{\min}\right)+6.26$	$0.58\log\left(\frac{P}{\min}\right)-1.17$
0.4 FM	$1.05\log\left(\frac{P}{\min}\right)+0.77$	$-0.30\log\left(\frac{P}{\min}\right)+4.92$	$-1.22\log\left(\frac{P}{\min}\right)+6.38$	$0.61\log\left(\frac{P}{\min}\right)-1.17$
0.7 FM	$1.05\log\left(\frac{P}{\min}\right)+0.98$	$-0.32\log\left(\frac{P}{\min}\right)+4.90$	$-1.28\log\left(\frac{P}{\min}\right)+6.54$	$0.64\log\left(\frac{P}{\min}\right)-1.13$
0.8 FM	$1.06\log\left(\frac{P}{\min}\right)+1.00$	$-0.32\log\left(\frac{P}{\min}\right)+4.89$	$-1.28\log\left(\frac{P}{\min}\right)+6.56$	$0.64\log\left(\frac{P}{\min}\right)-1.11$
0.9 FM	$1.08\log\left(\frac{P}{\min}\right)+1.02$	$-0.32\log\left(\frac{P}{\min}\right)+4.88$	$-1.28\log\left(\frac{P}{\min}\right)+6.57$	$0.64\log\left(\frac{P}{\min}\right)-1.09$
1.0 FM	$1.10\log\left(\frac{P}{\min}\right)+1.02$	$-0.32\log\left(\frac{P}{\min}\right)+4.87$	$-1.28\log\left(\frac{P}{\min}\right)+6.59$	$0.64\log\left(\frac{P}{\min}\right)-1.07$
1.1 FM	$1.12\log\left(\frac{P}{\min}\right)+1.02$	$-0.32\log\left(\frac{P}{\min}\right)+4.87$	$-1.28\log\left(\frac{P}{\min}\right)+6.60$	$0.64\log\left(\frac{P}{\min}\right)-1.06$
0.7 FO	$1.18\log\left(\frac{P}{\min}\right)+0.88$	$-0.30\log\left(\frac{P}{\min}\right)+4.84$	$-1.20\log\left(\frac{P}{\min}\right)+6.28$	$0.60\log\left(\frac{P}{\min}\right)-1.00$
0.8 FO	$1.17\log\left(\frac{P}{\min}\right)+0.93$	$-0.30\log\left(\frac{P}{\min}\right)+4.82$	$-1.20\log\left(\frac{P}{\min}\right)+6.29$	$0.60\log\left(\frac{P}{\min}\right)-0.98$
0.9 FO	$1.17\log\left(\frac{P}{\min}\right)+0.97$	$-0.30\log\left(\frac{P}{\min}\right)+4.81$	$-1.19\log\left(\frac{P}{\min}\right)+6.30$	$0.60\log\left(\frac{P}{\min}\right)-0.95$
1.0 FO	$1.17\log\left(\frac{P}{\min}\right)+1.01$	$-0.30\log\left(\frac{P}{\min}\right)+4.80$	$-1.19\log\left(\frac{P}{\min}\right)+6.31$	$0.60\log\left(\frac{P}{\min}\right)-0.93$
1.1 FO	$1.17\log\left(\frac{P}{\min}\right)+1.05$	$-0.30\log\left(\frac{P}{\min}\right)+4.79$	$-1.19\log\left(\frac{P}{\min}\right)+6.31$	$0.59\log\left(\frac{P}{\min}\right)-0.92$
Observed relations				
P24	$1.14_{\pm0.05}\log\left(\frac{P}{\min}\right)+0.50_{\pm0.20}$ [a]	$-0.08_{\pm0.01}\log\left(\frac{P}{\min}\right)+4.59_{\pm0.02}$ [b]	$-1.14_{\pm0.05}\log\left(\frac{P}{\min}\right)+6.30_{\pm0.07}$	$0.57_{\pm0.02}\log\left(\frac{P}{\min}\right)-1.19_{\pm0.04}$ [c]
This work[d]	-	$-0.08_{\pm0.02}\log\left(\frac{P}{\min}\right)+4.59_{\pm0.02}$	$-1.17_{\pm0.06}\log\left(\frac{P}{\min}\right)+6.33_{\pm0.08}$	$0.59_{\pm0.03}\log\left(\frac{P}{\min}\right)-1.20_{\pm0.04}$ [e]

[a] from $M_{\rm bol} = -2.85_{\pm0.12}\log\left(\frac{P}{\min}\right)+3.5_{\pm0.5}$ in P24

[b] Determined based on values in P24, i.e, based on 19 stars.

[c] Calculated assuming $M = 0.3\,M_\odot$ in $R = \sqrt{\frac{GM}{g}}$. For $M = 1.0\,M_\odot$, the relation is $0.57_{\pm0.02}\log\left(\frac{P}{\min}\right)-0.93_{\pm0.04}$

[d] Based on all available literature (observed BLAPs), i.e. 29 stars.

[e] Calculated assuming $M = 0.3\,M_\odot$ in $R = \sqrt{\frac{GM}{g}}$. For $M = 1.0\,M_\odot$, the relation is $0.59_{\pm0.03}\log\left(\frac{P}{\min}\right)-0.94_{\pm0.04}$

not yet been done, therefore in this study, we focus on the simplest parameter set A.

Overall, our results mostly favor the low-mass scenario (0.3 − 0.4 M$_\odot$) over the high-mass scenario (0.7 − 1.1 M$_\odot$) as the explanation for the evolutionary status of the majority of BLAPs. Nevertheless, it appears that (HG-)BLAPs consist of two to three groups of stars with differing physical parameters. Two explanations are possible: either they evolved to this point similarly, and we see a difference in their evolutionary stages as they cross the BLAP instability strip (high-mass scenarios of different L), or their physical origins are different (low vs high-mass models), but those different evolutionary scenarios converge to cross the BLAP instability region. Either way, only the high-mass scenario could correspond to the HG-BLAP subgroup. One of the main arguments is that in our models the lower mass scenario can only pulsate with the FM period and hence it causes the periods to become too long to match the HG-BLAPs.

The BLAP instability region is complicated and is potentially made up of multiple types of stars. This is highlighted by the fact that our work puts the only BLAP with a pulsation-based mass estimate (0.62 $M_\odot$) into the in-between region of proposed models. Our future work will involve non-linear modeling to compare theoretical light curves to observations which can tell us more about the models.

REFERENCES

Borowicz, J., Pietrukowicz, P., Mróz, P., et al. 2023a, AcA, 73, 1, doi: 10.32023/0001-5237/73.1.1

Borowicz, J., Pietrukowicz, P., Skowron, J., et al. 2023b, AcA, 73, 265, doi: 10.32023/0001-5237/73.4.2

Bradshaw, C. W., Dorsch, M., Kupfer, T., et al. 2024, MNRAS, 527, 10239, doi: 10.1093/mnras/stad3845

Byrne, C. M., & Jeffery, C. S. 2020, MNRAS, 492, 232, doi: 10.1093/mnras/stz3486

Byrne, C. M., Stanway, E. R., & Eldridge, J. J. 2021, MNRAS, 507, 621, doi: 10.1093/mnras/stab2115

Chang, S.-W., Wolf, C., Onken, C. A., & Bessell, M. S. 2024, MNRAS, 529, 1414, doi: 10.1093/mnras/stae637

Córsico, A. H., Romero, A. D., Althaus, L. G., Pelisoli, I., & Kepler, S. O. 2018, arXiv e-prints, arXiv:1809.07451, doi: 10.48550/arXiv.1809.07451

Gavras, P., Rimoldini, L., Nienartowicz, K., et al. 2023, A&A, 674, A22, doi: 10.1051/0004-6361/202244367

Heber, U. 2016, PASP, 128, 082001, doi: 10.1088/1538-3873/128/966/082001

Jermyn, A. S., Bauer, E. B., Schwab, J., et al. 2023, ApJS, 265, 15, doi: 10.3847/1538-4365/acae8d

Krtička, J., Krtičková, I., Bidin, C. M., et al. 2024, A&A, 683, A110, doi: 10.1051/0004-6361/202347359

Kupfer, T., Bauer, E. B., Burdge, K. B., et al. 2019, ApJL, 878, L35, doi: 10.3847/2041-8213/ab263c

Kupfer, T., Prince, T. A., van Roestel, J., et al. 2021, MNRAS, 505, 1254, doi: 10.1093/mnras/stab1344

Lin, J., Wang, X., Mo, J., et al. 2022, MNRAS, 509, 2362, doi: 10.1093/mnras/stab2812

—. 2023a, MNRAS, 523, 2172, doi: 10.1093/mnras/stad994

Lin, J., Wu, C., Wang, X., et al. 2023b, Nature Astronomy, 7, 223, doi: 10.1038/s41550-022-01783-z

McWhirter, P. R., & Lam, M. C. 2022, MNRAS, 511, 4971, doi: 10.1093/mnras/stac291

Meng, X.-C., Han, Z.-W., Podsiadlowski, P., & Li, J. 2020, ApJ, 903, 100, doi: 10.3847/1538-4357/abbb8e

Meng, X.-C., & Luo, Y.-P. 2021, MNRAS, 507, 4603, doi: 10.1093/mnras/stab2369

Nemec, J. M., Smolec, R., Benkő, J. M., et al. 2011, MNRAS, 417, 1022, doi: 10.1111/j.1365-2966.2011.19317.x

Netzel, H., Molnár, L., & Joyce, M. 2023, MNRAS, 525, 5378, doi: 10.1093/mnras/stad2611

Netzel, H., Pietrukowicz, P., Soszyński, I., & Wrona, M. 2022, MNRAS, 510, 1748, doi: 10.1093/mnras/stab3555

Netzel, H., & Smolec, R. 2022, MNRAS, 515, 3439, doi: 10.1093/mnras/stac1793

Paxton, B., Bildsten, L., Dotter, A., et al. 2011, ApJS, 192, 3, doi: 10.1088/0067-0049/192/1/3

Paxton, B., Cantiello, M., Arras, P., et al. 2013, ApJS, 208, 4, doi: 10.1088/0067-0049/208/1/4

Paxton, B., Marchant, P., Schwab, J., et al. 2015, ApJS, 220, 15, doi: 10.1088/0067-0049/220/1/15

Paxton, B., Schwab, J., Bauer, E. B., et al. 2018, ApJS, 234, 34, doi: 10.3847/1538-4365/aaa5a8

Paxton, B., Smolec, R., Schwab, J., et al. 2019, ApJS, 243, 10, doi: 10.3847/1538-4365/ab2241

Petersen, J. O. 1973, A&A, 27, 89

Pietrukowicz, P., Dziembowski, W. A., Latour, M., et al. 2017, Nature Astronomy, 1, 0166, doi: 10.1038/s41550-017-0166

Pietrukowicz, P., Latour, M., Soszynski, I., et al. 2024, arXiv e-prints, arXiv:2404.16089, doi: 10.48550/arXiv.2404.16089

Pigulski, A. 2014, in Precision Asteroseismology, ed. J. A. Guzik, W. J. Chaplin, G. Handler, & A. Pigulski, Vol. 301, 31–38, doi: 10.1017/S1743921313014038

Pigulski, A., Kotysz, K., & Kołaczek-Szymański, P. A. 2022, A&A, 663, A62, doi: 10.1051/0004-6361/202243293

Prudil, Z., Smolec, R., Skarka, M., & Netzel, H. 2017, MNRAS, 465, 4074, doi: 10.1093/mnras/stw3010

Ramsay, G. 2018, A&A, 620, L9, doi: 10.1051/0004-6361/201834604

Ramsay, G., Woudt, P. A., Kupfer, T., et al. 2022, MNRAS, 513, 2215, doi: 10.1093/mnras/stac1000

Rimoldini, L., Holl, B., Gavras, P., et al. 2023, A&A, 674, A14, doi: 10.1051/0004-6361/202245591

Romero, A. D., Córsico, A. H., Althaus, L. G., Pelisoli, I., & Kepler, S. O. 2018, MNRAS, 477, L30, doi: 10.1093/mnrasl/sly051

Smolec, R., Dziembowski, W., Moskalik, P., et al. 2017, in European Physical Journal Web of Conferences, Vol. 152, European Physical Journal Web of Conferences, 06003, doi: 10.1051/epjconf/201715206003

Smolec, R., Moskalik, P., Plachy, E., Soszyński, I., & Udalski, A. 2018, MNRAS, 481, 3724, doi: 10.1093/mnras/sty2452

Smolec, R., Prudil, Z., Skarka, M., & Bakowska, K. 2016, MNRAS, 461, 2934, doi: 10.1093/mnras/stw1519

Soszyński, I., Udalski, A., Szymański, M. K., et al. 2015, AcA, 65, 297, doi: 10.48550/arXiv.1601.01318

—. 2016, AcA, 66, 131, doi: 10.48550/arXiv.1606.02727

Soszyński, I., Udalski, A., Wrona, M., et al. 2019, AcA, 69, 321, doi: 10.32023/0001-5237/69.4.2

Soszyński, I., Udalski, A., Szymański, M. K., et al. 2020, AcA, 70, 101, doi: 10.32023/0001-5237/70.2.2

Udalski, A., Szymański, M. K., & Szymański, G. 2015, AcA, 65, 1, doi: 10.48550/arXiv.1504.05966

Udalski, A., Soszyński, I., Pietrukowicz, P., et al. 2018, AcA, 68, 315, doi: 10.32023/0001-5237/68.4.1

Wu, T., & Li, Y. 2018, MNRAS, 478, 3871,

  doi: 10.1093/mnras/sty1347

Xiong, H., Casagrande, L., Chen, X., et al. 2022, A&A, 668, A112,
  doi: 10.1051/0004-6361/202244571

Zhang, X., Jeffery, C. S., Su, J., & Bi, S. 2023, ApJ, 959, 24,
  doi: 10.3847/1538-4357/ad0a65

APPENDIX

A. INLIST USED

An example inlist used for linear computations of the models using the convection parameter set A is provided below.

```
! inlist_rsp_blap to estimate new theoretical instability regions for BLAPs
! Contributors: D. Jadlovský, S. Das and L. Molnár

&star_job

      show_log_description_at_start = .false.

      create_RSP_model = .true.

      save_model_when_terminate = .true.
      save_model_filename = 'final.mod'

      initial_zfracs = 6

      color_num_files=2
      color_file_names(2)='blackbody_johnson.dat'
      color_num_colors(2)=5

      set_initial_age = .true.
      initial_age = 0

      set_initial_model_number = .true.
      initial_model_number = 0

      set_initial_cumulative_energy_error = .true.
      new_cumulative_energy_error = 0d0

      !pgstar_flag = .true.

      !relax_initial_composition=.true.


/ ! end of star_job namelist

&eos
use_PC = .true.
use_Skye = .false.
!finished_relax = .false.

/

&kap
      Zbase    = 0.05d0

      kap_file_prefix = 'a09'
      kap_lowT_prefix = 'lowT_fa05_a09p'
```

```
      kap_CO_prefix = 'a09_co'

/ ! end of kap namelist

&controls

   max_model_number = 2

! RSP controls

   ! possible model for BLAP pulsations
   RSP_X    =    0.7d0
   RSP_Z    =    0.05d0

   RSP_use_Prad_for_Psurf = .true.

   ! initial kick velocity-amplitude
   RSP_kick_vsurf_km_per_sec = 0.5d0
   !RSP_fraction_1st_overtone = 0d0
   !RSP_fraction_2nd_overtone = 0d0

   ! controls for building the initial model
   RSP_nz       = 280  ! total number of zones in initial model
   RSP_nz_outer = 140  ! number of zones in outer region of initial model
   RSP_T_anchor = 2d5  ! approx temperature at base of outer region
   RSP_T_inner  = 6d6  ! T at inner boundary of initial model

   RSP_alfa   =    1.5d0         ! mixing length; alfa = 0 gives a purely radiative model.
   RSP_alfac  =    1.0d0         ! convective flux; Lc ˜ RSP_alfac
   RSP_alfas  =    1.0d0         ! turbulent source; Lc ˜ 1/ALFAS; PII ˜ RSP_alfas
   RSP_alfad  =    1.0d0         ! turbulent dissipation; damp ˜ RSP_alfad
   RSP_alfap  =    0.0d0         ! turbulent pressure; Pt ˜ alfap
   RSP_alfat  =    0.0d0         ! turbulent flux; Lt ˜ RSP_alfat; overshooting.
   RSP_alfam  =    0.25d0        ! eddy viscosity; Chi & Eq ˜ RSP_alfam
   RSP_gammar =    0.0d0         ! radiative losses; dampR ˜ RSP_gammar

   ! artificial viscosity controls
   ! for the equations see: Appendix C in Stellingwerf 1975
   ! http:\\adsabs.harvard.edu/abs/1975ApJ...195..441S.
   ! In principle, for not too-non-adiabatic convective models artificial viscosity is not
   ! needed or should be very small. Hence a large cut-off parameter below (in purely
   ! radiative models the default value for cut-off was 0.01)
   RSP_cq  = 1.0d0     ! canonical 4.0
   RSP_zsh = 0.1d0     ! canonical 0.1


   ! the following relate to stage 1, creating the initial model
   RSP_max_outer_dm_tries = 200 ! give up if fail to find outer dm in this many attempts
   RSP_max_inner_scale_tries = 100
            ! give up if fail to find inner dm scale factor in this many attempts
   RSP_T_anchor_tolerance = 1d-8
            ! allowed relative difference between T at base of outer region and T_anchor
```

```
RSP_T_inner_tolerance = 1d-8
          ! allowed relative difference between T at inner boundary and T_inner

  ! these are for stage 2, the \relaxing" of the initial envelope created in stage 1.
  RSP_relax_initial_model = .false.     !! .false. might be necessary for some model settings afg/2019
  RSP_relax_alfap_before_alfat = .true. ! else reverse the order
  RSP_relax_max_tries = 1000
  RSP_relax_dm_tolerance = 1d-6   !canoncial 1d-6
  ! the final control, RSP_relax_dm_tolerance, may be your best chance for getting
  ! around the problem you reported

! solver
   use_gold2_tolerances = .true.


/ ! end of controls namelist
```

B. ADDITIONAL LNA FIGURES

In Fig. 5 we show the effects of different convection parameter sets on the shape of the instability strip.
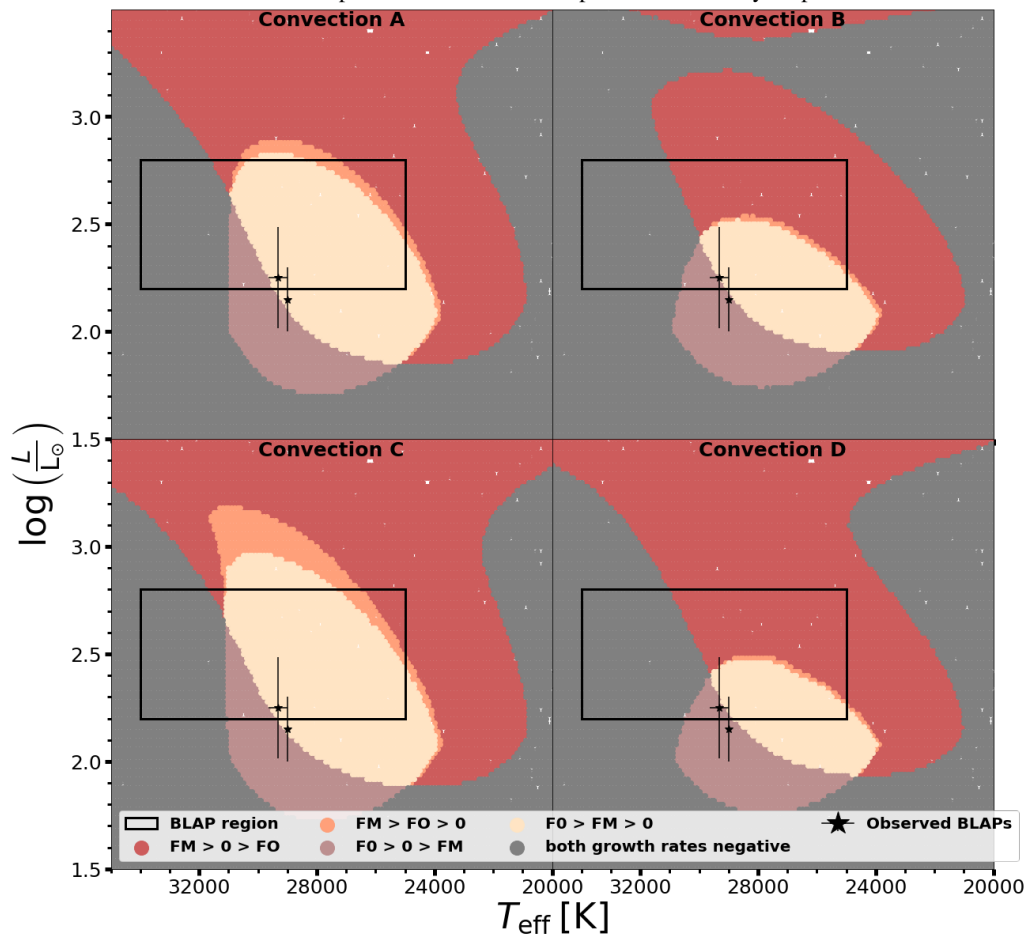

Figure 5. Same as in Fig. 1 but demonstrating the effects of convection parameter sets for the case of $M = 1.1\,M_\odot$. We find that the choice of convective parameters significantly affects the growth rates in different pulsation modes.